Influence of Co/Fe molar ratio on hydrotalcite catalysts prepared with or without microwave

Cynthia Abou Serhal, Rebecca El Khawaja, Madona Labaki, Isabelle Mallard, Christophe Poupin, Renaud Cousin, Stéphane Siffert

Version of Record: https://www.sciencedirect.com/science/article/pii/S0022459622000676
Manuscript_9cbc139d7d5cb4c94dc6960e038aacc3

Influence of Co/Fe molar ratio on hydrotalcite catalysts prepared with or without microwave

Cynthia Abou Serhal[a,b], Rebecca El Khawaja[a], Madona Labaki[b], Isabelle Mallard[a], Christophe Poupin[a], Renaud Cousin[a*], Stéphane Siffert[a*]

a Université du Littoral Côte d'Opale (ULCO), Unité de Chimie Environnementale et Interactions sur le Vivant (UCEIV, U.R. 4492), SFR Condorcet FR CNRS 3417, MREI, F-59140 Dunkerque, France

b Lebanese University, Laboratory of Physical Chemistry of Materials (LCPM)/PR2N, Faculty of Sciences, Fanar, P.O. Box 90656, Jdeidet El Metn, Lebanon

* Corresponding authors. E-mail addresses: stéphane.siffert@univ-littoral.fr; renaud.cousin@univ-littoral.fr; Tel.: +33-03-2865-8256; +33-03-2865-8276.

Abstract

Two series of mixed cobalt-iron oxides were synthesized by the conventional hydrotalcite route, without (Co_xFe_2-HT) or with microwave irradiations (Co_xFe_2-MW). Different molar ratios Co^{2+}/Fe^{3+} were also investigated with $2 \leq x \leq 8$. X-ray diffraction (XRD) analysis confirmed the formation of the desired hydrotalcite phase for all the materials before calcination whatever the molar ratio Co^{2+}/Fe^{3+} is. After calcination of the latter materials at 500 °C, XRD evidenced the complete destruction of the hydrotalcite phase and, consequently, the formation of mixed oxides of cobalt and iron.
After being characterized, the oxides materials were tested towards the total oxidation of the volatile organic compound (VOC) propene. Both the molar ratio and the preparation method have a significant effect on the catalytic properties. The light-off curves of Co_xFe_2-HT500 materials showed that the catalytic activity is improved for a molar ratio $Co^{2+}/Fe^{3+} > 2$. Co_6Fe_2-HT500, with the ratio Co^{2+}/Fe^{3+} equal to 3, showed the best catalytic performance. Furthermore, except for Co_8Fe_2-MW500, the materials that were subjected to microwave irradiations gave higher catalytic activities compared to those of the homologous ones prepared without such irradiations. Co_6Fe_2-MW500 was found to be the most catalytically active among all the materials of both series due to the higher specific surface area, the higher amount and easier reducibility of active species, higher proportion of mobile oxygen and of Co^{2+} on the surface. Furthermore, this catalyst did not show tendency to deactivation and coking even after 100 h under stream.

Keywords: Mixed cobalt-iron oxides; Hydrotalcite-like materials; Microwave irradiation; Molar ratio; Catalytic oxidation

1. Introduction

Heterogeneous catalysis is regarded as one of the most promising strategies for volatile organic compounds (VOCs) removal that consists in the oxidation of VOCs into carbon dioxide (CO_2) and water (H_2O) in the presence of a catalyst according to the following reaction:

$$4\ C_xH_yO_z + (4x + y - 2z)\ O_2 \rightarrow 4x\ CO_2 + 2y\ H_2O$$

This technique has triggered tremendous interest in the past two decades and made huge progress and developments [1] in order to understand the influence of the catalyst used (composition, nature, synthesis, design…) during the VOC oxidation.

Among the most studied metal oxides, catalysts based on cobalt oxide are generally the most used and now the most active in the catalytic oxidation of VOCs. Indeed, the high activity of this oxide resides in its high reduction capacity. The relatively weak Co-O bond, generates an easy interaction between the oxygen atoms of the lattice and the reagents of the oxidation reaction [2]. This redox property is often sought after, since the Mars-Van Krevelen mechanism takes place usually in these reactions [3]. Several factors influence the properties and the catalytic performance of cobalt species. Indeed, Xie et al. [4] evaluated the catalytic performance of o-xylene oxidation, while Bai et al. [5] and Li et al. [6] tested a mesoporous compound for the oxidation of toluene. These three groups of authors found better activity for mesoporous Co_3O_4 species than for bulk Co_3O_4.

Mesoporous materials have a developed and organized pore structure, which is advantageous in giving more accessible active sites for the reactive molecule. Moreover, mesoporous Co_3O_4 with different structures and morphologies were prepared in presence of hard templates (MCM-48, MCM-41 and SBA-15) by Yu et al. [7]. In this study, the material with the largest surface area showed the highest catalytic performance. Other studies revealed that soft templates can also be effective for the synthesis of Co_3O_4 materials with remarkable physicochemical properties [8,9]. For example, the inverse micelle method appeared to be effective for the synthesis of unique pore structure Co_3O_4 based material for 2-propanol oxidation [10]. The increase in catalytic performance is essentially associated with a higher specific surface area, greater abundance of Co^{3+} active species and higher number of surface oxygen, and better reducibility of oxide species. Several studies have succeeded in increasing the dispersion of cobalt species using different supports. Indeed, Carrillo et al. [2] used halloysite clay support, and showed that for monometallic catalysts, the cobalt-based catalyst exhibits better toluene oxidation performance than the copper-based catalyst. Mei et al. [11] have found that the highest activity towards dibromomethane oxidation in the presence of Co_3O_4/CeO_2 catalyst is related to the high content of Co^{3+} and surface oxygen. In addition, it has been found that Co_3O_4 supported on clinoptilolite-type zeolite gives good catalytic activity towards toluene oxidation [12]. Konsolakis et al. [13] reported that the introduction of cobalt with cerium oxide remarkably increases the catalytic activity towards ethyl acetate oxidation. On the other hand, nanocrystalline cobalt oxide showed higher activity than supported catalysts towards propane oxidation [14]. Luo et al. [15] studied the influence of cobalt and manganese binary oxides on the total oxidation of toluene and found that the molar ratio Co/Mn = 1 has the best catalytic activity. In fact, the highest activity

towards the oxidation of toluene is related to the concentrations of active cobalt species at the surface.

Another transition metal, that has triggered interest for its ecological property and low cost, is iron metal oxide [16] that also presents high sintering temperature that can prevent catalytic deactivation. Indeed, Tseng et al. [17] obtained excellent catalytic performances for iron oxide catalysts (MnO/Fe_2O_3) for the total oxidation of styrene. Similarly, Kim et al. [18] studied the influence of iron-based catalysts. The following catalytic order shows that iron metal has the highest performance towards the total oxidation of hexane: $LaFeO_3 > LaCoO_3 > LaMnO_3 > PdO/Al_2O_3$. In addition, the influence of the preparation method was investigated. It was found that iron prepared by the co-precipitation method showed better catalytic activity towards toluene oxidation than the one prepared by impregnation [19]. On the other hand, the most efficient iron catalyst also exhibited a high thermal stability for at least 30 hours. Similarly, a comparison was made by Li et al. [20] on aluminum and iron catalysts introduced on montmorillonites. The researchers found that the iron-based catalysts had higher catalytic performance and thermal stability towards the total oxidation of toluene and chlorobenzene than those of the aluminum catalysts. Furthermore, it has been found that a higher concentration of iron in the lamellar material enhances the catalytic reactivity of these VOCs.

We have previously investigated [21] the importance of the hydrotalcite route [22] in order to obtain a well dispersed transition mixed oxides based on Co, Mg, Al, and Fe prepared as catalysts towards the total oxidation of VOC. It has been proved that the mixed cobalt-iron oxide $Co_4Fe_2O_7$ exhibited the best catalytic activity among the studied solids. In addition, we have reported the advantage of microwave irradiations as an unconventional synthesis method for hydrotalcite preparation [23]. Moreover, we have investigated the influence of different microwave irradiation parameters (temperature, power, and time) used during this synthesis, on the performance of the mixed cobalt-iron oxides towards the total oxidation of the VOC propene [24].
It is well known that the molar cationic ratio influences the formation of hydrotalcite-like materials. In order to obtain pure hydrotalcite phase, the molar ratio M^{2+}/M^{3+} must be in the range of 2 to 4 [25]. Indeed, the effect of molar ratio on the formation of hydrotalcite-like materials was reported by many authors [26]. The effect of the molar cationic ratio in the range of 0.5 to 3, was investigated for Cu/Al hydrotalcite-like materials. The highest crystallinity was obtained for the sample Cu/Al with the molar ratio equal to 1. The decrease of the Cu/Al molar ratio promotes a decrease of malachite crystallinity [27]. In addition, Abderrazek et al. [28] showed that the molar ratio influences the crystallinity and the purity of the hydrotalcite-like materials. In fact, the synthesized sample Zn/Al with a molar ratio equal to 2, showed the highest intensities in XRD patterns compared to other samples with molar ratios between 1 and 5. Similarly, the increase of Zn/Al molar ratio leads to a decrease in intensities and sharpness of XRD peaks. It was due to the formation of other crystallite phases such as ZnO and $ZnAl_2O_4$ [29,30].
The aim of this paper is to investigate the influence of the molar ratio Co^{2+}/Fe^{3+} and the preparation method, with or without microwave, of Co/Fe hydrotalcite-like materials on the catalytic oxidation of the VOC propene.

2. Experimental

2.1. Catalysts synthesis

Several hydrotalcite-like samples containing different amounts of Co and Fe cations were prepared by the co-precipitation method. The solids were prepared by mixing an aqueous solution containing appropriate amounts of $Co(NO_3)_2.3H_2O$ (CHEM-LAB purity 97 %) and $Fe(NO_3)_3.9H_2O$ (CHEM-LAB, purity 98 %) depending on the desired molar ratio Co^{2+}/Fe^{3+} = 1; 2; 3 or 4. The solution was added dropwise at room temperature, into a stirred 1 $mol.L^{-1}$ sodium carbonate (ACROS, 99.5 %) solution. The pH was kept at a constant value of 10 using 2 $mol.L^{-1}$ sodium hydroxide (PANREAC, 98 %) solution.

After complete precipitation, half of the solution was left under vigorous stirring for 24 h at 60 °C, while the other half was submitted to microwave irradiation for 1 min at 40 W (38 °C). These microwave parameters were evaluated and optimized in our previous work [24].

At last, all samples were filtered, washed with hot deionized water until neutralization, and dried for 48 h. The obtained precipitates were ground and calcined under an air flow (2 $L.h^{-1}$, 1 $°C.min^{-1}$) at 500 °C for 4 h. Uncalcined samples will be denoted as Co_xFe_2-HT and Co_xFe_2-MW, where HT and MW represent the conventional and microwave treatment respectively, whereas the subscript x represents the molar ratio of cobalt metal with x = 2; 4; 6 and 8. The samples calcined at 500 °C will be designated by Co_xFe_2-HT500 and Co_xFe_2-MW500.

2.2. Characterization techniques

Element chemical analyses for Co and Fe were carried out using Inductively Coupled Plasma-Optical Emission Spectrometer (ICP OES, Thermo ICAP 6300 DUO).

Structural analysis of the different catalysts was carried out at room temperature by powder X-ray diffraction (XRD). The patterns were recorded using a Bruker D8 advance diffractometer, with a copper anode CuK_α radiation (λ = 1.5418 Å). The measurements were taken from 5 to 80° with a step size of $\Delta(2\theta)$ = 0.02 and a counting time of 2 s per step. Identification of the crystalline phases was made with the Joint Committee on Powder Diffraction Standards (JCPDS) files, using EVA software.

The specific surface area was calculated by Brunauer-Emmett-Teller (BET) method, by nitrogen adsorption at low temperature (-196 °C), using ANKERSMIT Quanta Sorb Junior apparatus. Before the adsorption, the uncalcined samples were degassed at 60 °C for 45 min and the calcined samples at 130 °C for 30 min.

The reducibility of the calcined samples was studied by temperature-programmed reduction method (H_2-TPR). Experiments were carried out in an Altamira AMI 200 apparatus starting from room temperature to 950 °C, with a heating rate of 5 $°C.min^{-1}$. H_2-TPR runs were carried out in a flow (30 $mL.min^{-1}$) of 5 vol.% H_2 diluted in argon. The evolution of hydrogen consumption was detected by a thermal conductivity detector (TCD).

X-ray photoelectron spectroscopy (XPS) analyses were conducted on a Kratos Axis Ultra spectrometer with a monochromatic Al *K*α (hν = 1486.6 eV) radiation source and a

hemispherical analyzer with constant ΔE/E. The power of the source was maintained at 150 W. The binding energy (BE) was calibrated based on the line position of C 1s (285 eV). The simulations and the quantifications of the data were carried out on the CasaXPS software.

Thermal decomposition analyzes were performed on a SDT Q600 device operated under an air flow of 100 mL.min^{-1}. The sample (about 15 mg) was heated from room temperature to 1000 °C with a heating rate of 5 °C.min^{-1}. The results obtained were treated using T.A. UNIVERSAL ANALYSIS software.

2.3. Catalytic test

The total oxidation of propene reaction was performed at atmospheric pressure in a continuous flow fixed bed reactor with 10 mm of inner diameter. 100 mg of catalyst were used. The catalyst was pretreated under an air flow at 150 °C for 1 h. The reaction was then studied in temperature range 150 - 500 °C with an increase of 1 °C.min^{-1}. Two thermocouples were used: one inside the furnace and another placed near to the catalytic bed in order to control and monitor the temperature during the test. A total flow rate of 100 mL.min^{-1} composed of 6000 pm propene balanced by air was studied. The reactants and the oxidation products were then analyzed using a Varian CP-4900 microGC coupled with a TCD detector. The catalytic performance of the synthesized materials was evaluated based on the temperature at which 50% of the propene was converted into CO_2, which will be affiliated to T_{50} in this presented work. The propene conversion was defined as a function of carbon number of the products and eventual by-products of this oxidation reaction:

$$Propene\ conversion\ (\%) = \frac{(\%CO_2)_t + (\%CO)_t}{(\%CO_2)_t + (\%CO)_t + 3 \times (\%C_3H_6)_t} \times 100$$

3. Results and discussion

3.1. Characterization

Table 1. Chemical analysis, cell parameters (a and c), and specific surface areas of the uncalcined samples

Sample	Chemical analysis		a* (Å)	c** (Å)	Specific surface area ($m^2.g^{-1}$)
	Theoretical	Experimental			
Co_2Fe_2-HT	1	1.01	3.12	22.57	63
Co_2Fe_2-MW	1	1.03	3.12	22.08	70
Co_4Fe_2-HT	2	2.05	3.11	22.65	68
Co_4Fe_2-MW	2	2.04	3.11	22.19	91

Co_6Fe_2-HT	3	3.03	3.12	23.13	76
Co_6Fe_2-MW	3	3.02	3.12	23.16	111
Co_8Fe_2-HT	4	4.08	3.11	23.08	60
Co_8Fe_2-MW	4	4.07	3.10	23.07	45

* a = 2 x $d_{(110)}$ ** c = 3 x $d_{(003)}$

The ICP results presented in Table 1 show that the experimental molar ratios Co^{2+}/Fe^{3+} are very close to those desired, for the two preparation methods, thus validating the syntheses carried out with the various molar ratios going from 1 to 4.

The XRD patterns of the uncalcined CoFe samples prepared with or without microwave irradiations are presented in Fig. 1.

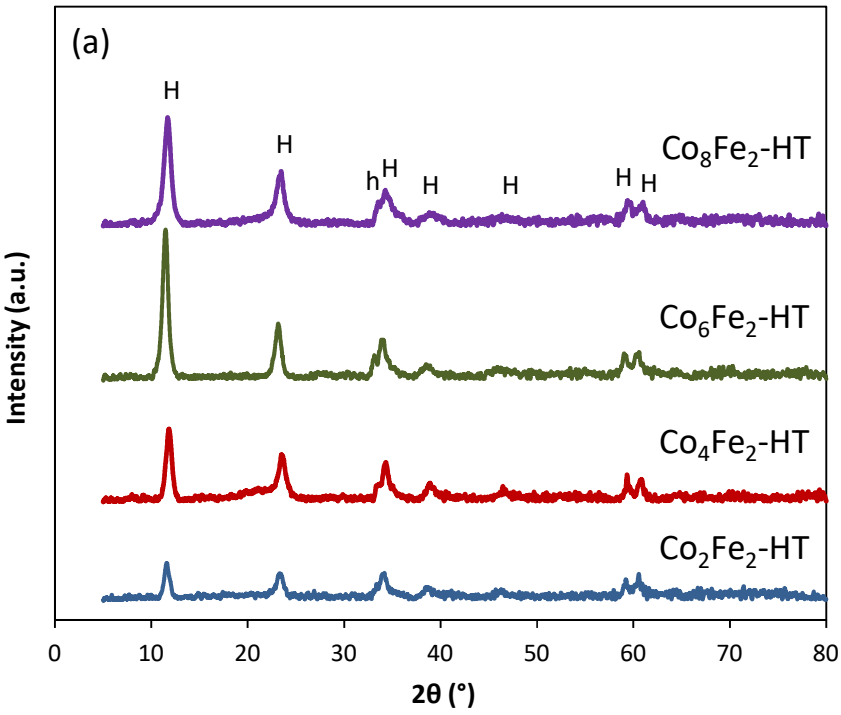

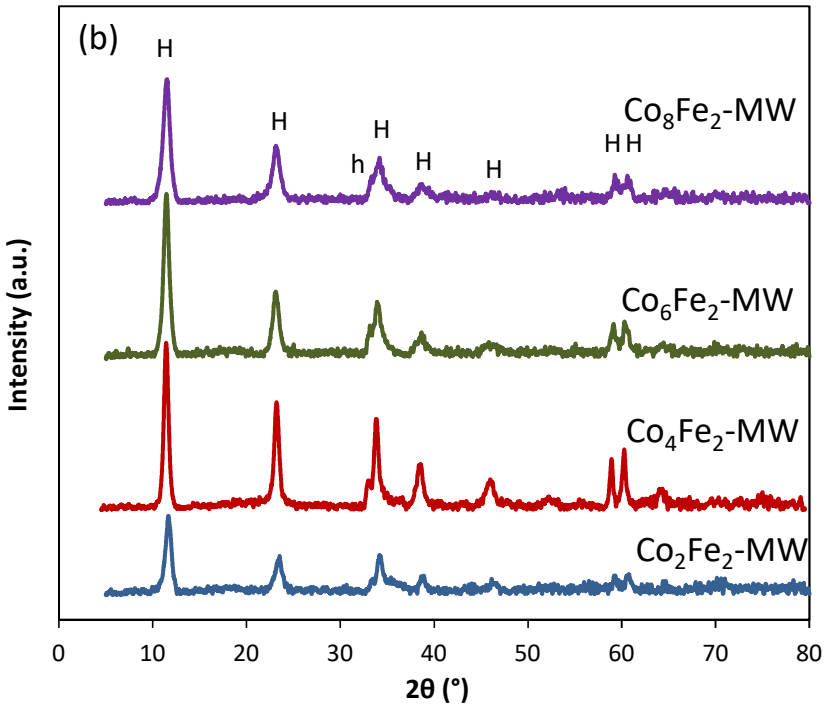

Fig. 1. X-ray diffraction patterns of the uncalcined samples prepared with different Co/Fe molar ratios. (a) Co_xFe_2-HT samples; (b) Co_xFe_2-MW samples. H: Hydrotalcite phase (JCPDS No.50-0235);
h: Cobalt hydroxide α-$Co(OH)_2$ (JCPDS No. 46-0605)

The patterns obtained correspond to the rhombohedral hydrotalcite phase belonging to the space group [31], similar to $Co_{5.84}Fe_{2.16}(OH)_{16}(CO_3)_{1.08}.0.32H_2O$ (JCPDS-ICDD 50-0235) [32], having cobalt as the divalent cation and iron as the trivalent cation. The comparison of XRD patterns indicates a difference in the intensities of the lines of the hydrotalcite phase (H) by modifying the ratio between the divalent cation Co^{2+} and the trivalent cation Fe^{3+}. Moreover, a minor phase of cobalt hydroxide α-$Co(OH)_2$ was detected at approximately $2\theta = 33.5$ ° [33]. Despite the decrease in the cobalt content by decreasing the Co^{2+}/Fe^{3+} molar ratio, this phase is still detected for both Co_2Fe_2-HT and Co_2Fe_2-MW solids. According to Ma et al. [32], the incorporation of iron has prevented the formation of β-$Co(OH)_2$, unlike the hydrotalcite containing cobalt where a mixture of both α-$Co(OH)_2$ and β-$Co(OH)_2$ was detected.

The crystallographic parameters “a” and “c” of the dried solids determined by XRD measurements are listed in Table 1. As predicted, the increase in the Co^{2+}/Fe^{3+} ratio does not cause any remarkable difference for the “a” parameter for both series of samples, since the crystallographic parameter “a” corresponds to the average cation-cation (Co^{2+}-Fe^{3+}) distance in a hydroxide sheet.
Concerning the crystallographic parameter “c” which gives information on the thickness of the interlayer domain [34], an increase of this parameter is noticed when the ratio Co^{2+}/Fe^{3+} increases. As a result, Co_6Fe_2 and Co_8Fe_2 samples have the highest c values.

Similarly, Pérez Bernal et al. [35] also reported a slight increase in the "c" parameter with the increase in the Co^{2+}/Fe^{3+} ratio prepared by the conventional hydrotalcite method, and thus when the Fe^{3+} content decreases.
Moreover, the increase of the parameter "c" with the increase of the Co^{2+}/Fe^{3+} ratio can be attributed on one hand to the substitution of Fe^{3+} by Co^{2+} ions leading to a decrease in the positive charge density of the brucite-like sheet, thus reducing the electrostatic interaction between the brucite layer and the interlayer domain [36]. On the other hand, the high cobalt content could cause partial oxidation of Co^{2+} ions to Co^{3+} during synthesis. The highest oxidation state of Co^{3+} requires more carbonate for charge compensation in the interlayer domain, hence the higher value of the parameter "c". The partial oxidation of Co^{2+} to Co^{3+} during synthesis has also been observed and reported by other authors [37–39].

The specific surface areas of the two series of samples before calcination at 500 °C are shown in Table 1. In fact, the specific surface areas vary not only according to the nature of the cations present in the hydrotalcite structure but also depend on the ratio of the cations and the preparation method. First, the dried solids showed that with the increase of the Co^{2+}/Fe^{3+} ratio from 1 to 3, the specific surface values increase. The highest specific surface area was obtained for the sample with Co^{2+}/Fe^{3+} ratio of 3, in particular for the Co_6Fe_2-MW solid, with a specific surface area equal to 111 $m^2.g^{-1}$. These results are in agreement with those of Rives et al. [40] for hydrotalcite (Cu+Co)/Al solids. Indeed, an increase of the specific surface area is obtained with the increase of the cobalt content. Changes in morphology are behind these observations. On the other hand, a decrease in the specific surface area is observed when the molar ratio Co^{2+}/Fe^{3+} increases from 3 to 4. It is worth mentioning that all specific surface areas of Co_xFe_2-MW dried samples are higher than those of the conventional series Co_xFe_2-HT. However, for a molar ratio of 4, a lower specific surface area is obtained for the MW sample (45 $m^2.g^{-1}$ for Co_8Fe_2-MW) compared to that of the conventional one (60 $m^2.g^{-1}$ for Co_8Fe_2-HT).

The XRD patterns of the Co_xFe_2-HT500 and Co_xFe_2-MW500 solids are presented in Fig. 2(a) and Fig. 2(b) respectively.

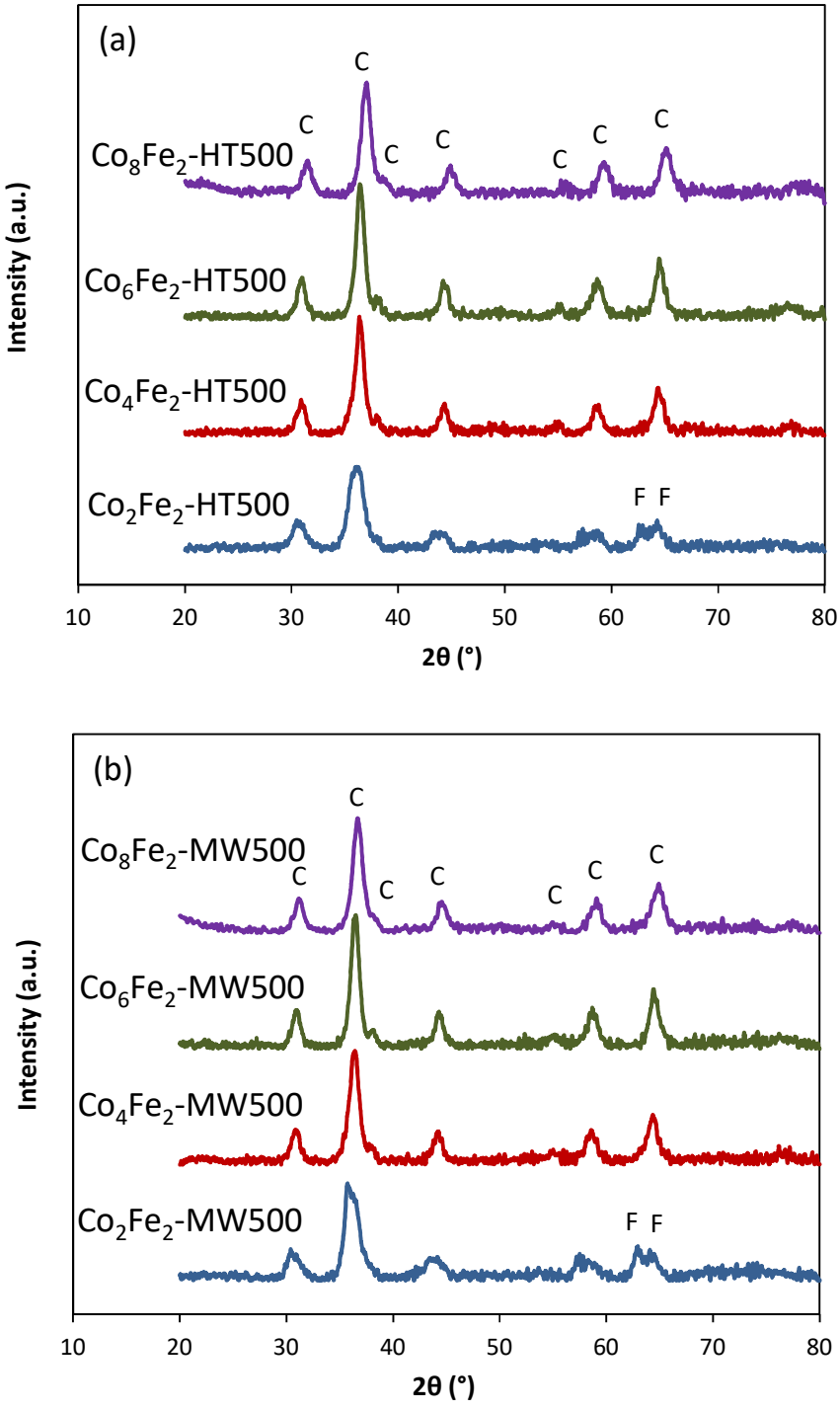

Fig. 2. X-ray diffraction patterns of the calcined samples prepared with different Co/Fe molar ratios. (a) Co_xFe_2-HT500 samples; (b) Co_xFe_2-MW500 samples. C: Co_3O_4 (JCPDS No. 42-1467) and $CoFe_2O_4$ (JCPDS No. 22-1086); F: ɤ-Fe_2O_3 (JCPDS N° 04-0755)

It is obvious that the hydrotalcite structure is destroyed after the heat treatment. The new crystalline phases are attributed to mixed oxides of cobalt and iron. For both series of samples, the presence of Co_3O_4 and $CoFe_2O_4$ phases is noted.
The XRD patterns for the Co_2Fe_2-HT500 and Co_2Fe_2-MW500 samples show the presence of a new phase corresponding to γ-Fe_2O_3 at $2\theta° = 62°$ and $64°$ [41]. Indeed, these samples have the lowest ratio Co^{2+}/Fe^{3+}, and therefore the highest iron content. As a result, the formation of iron oxide may be due to the higher iron content present in these solids [42].

Table 2. Specific surface areas and temperature at 20% (T_{20}) and 50% (T_{50}) propene conversion of the oxides catalysts

Sample	Specific surface area ($m^2.g^{-1}$)	T_{20} (°C)	T_{50} (°C)
Co_2Fe_2-HT500	58	228	232
Co_2Fe_2-MW500	60	234	237
Co_4Fe_2-HT500	57	242	244
Co_4Fe_2-MW500	80	212	214
Co_6Fe_2-HT500	79	209	213
Co_6Fe_2-MW500	95	195	200
Co_8Fe_2-HT500	56	220	224
Co_8Fe_2-MW500	28	246	280

After calcination at 500 °C, the oxides formed have lower specific areas than the dried samples, except for Co_6Fe_2-HT500 which has a slightly higher surface area after calcination (Table 2). Furthermore, all Co_xFe_2-MW500 samples have higher specific surface areas than the Co_xFe_2-HT500 series, especially for solids with a molar ratio of 2 and 3. However, the solid with a molar ratio $Co^{2+}/Fe^{3+} = 4$ is an exception, since Co_8Fe_2-MW500 (28 $m^2.g^{-1}$) shows a lower specific surface area than Co_8Fe_2-HT500 (56 $m^2.g^{-1}$). The isotherms obtained for all samples (shown in Supplementary Information Fig.S1.) are of type IV, based on the IUPAC classification, attributed to mesoporous materials. Solids resulting from both syntheses present a hysteresis loop of type H1 with a plateau at high P/P_0 often associated with agglomerates that result in a narrow pore size distribution.

Temperature-programmed reduction (H_2-TPR) experiments showed two reduction peaks for all Co_xFe_2-HT500 and Co_xFe_2-MW500 samples. The profiles (shown in supplementary data Fig.S2.) are similar to those obtained in our previous works [21,24]. It is important to note that for all TPR profiles of mixed Co-Fe oxides synthesized with different ratios, the first peak is attributed to the reduction of Co_3O_4 to CoO [43,44]. The second intense peak, at higher temperature, corresponds to the reduction of CoO to metallic cobalt (Co^0) as well as to the simultaneous reduction of Fe_2O_3 to Fe_3O_4 and Fe^0

[45,46]. It is known that the reduction of cobalt and iron oxides takes place at quite different temperatures. It has been previously reported that the reduction of two oxides incorporated on the same support occurs simultaneously, even though their reductions take place at different temperatures when they are not in presence of each other. In fact, it is assumed that hydrogen is dissociatively adsorbed on the cobalt particles, with a spillover of the hydrogen atoms, leading to a decrease of the reduction temperature of the iron oxide particles [47].

Table 3. Theoretical and experimental hydrogen consumptions and maximum reduction temperature of each oxide sample

Sample	Theoretical H_2 consumption (µmol $H_2.g^{-1}_{cata}$)			Maximum reduction temperature (°C)		Experimental H_2 consumption (µmol $H_2.g^{-1}_{cata}$)
	Co_3O_4 into Co^0	Fe_2O_3 into Fe^0	Total	1st peak	2nd peak	
Co_2Fe_2-HT500	8614	9691	18305	330	483	17254
Co_2Fe_2-MW500				318	451	17324
Co_4Fe_2-HT500	11608	6530	18138	291	409	16622
Co_4Fe_2-MW500				280	401	18329
Co_6Fe_2-HT500	13129	4924	18053	279	413	18330
Co_6Fe_2-MW500				262	400	18450
Co_8Fe_2-HT500	14051	3952	18003	299	427	16288
Co_8Fe_2-MW500				313	425	15265

It is noted that increasing the Co^{2+}/Fe^{3+} molar ratio from 1 to 3, results in a shift of the reduction peaks to lower temperatures (Table 3). This indicates that the increase in cobalt content induces an easier reducibility of the oxide species [42]. However, by a further increase of the ratio to 4, an increase in the reduction temperatures is observed. Indeed, Co_8Fe_2-HT500 shows reduction peaks at temperatures higher than those of Co_4Fe_2-HT500 and Co_6Fe_2-HT500.

In addition, Co_xFe_2-MW500 series, except for Co_8Fe_2-MW500, exhibit lower reduction temperatures than those of their homologues Co_xFe_2-HT500. Furthermore, the experimental values of hydrogen consumed, which are close to the theoretical ones, suggest that almost all of cobalt and iron oxides in the studied samples are reduced under our experimental conditions

3.2. Catalytic performance and X-ray photoelectron spectroscopy (XPS)

Fig. 3 displays the evolution of propene conversion to CO_2 versus the reaction temperature in the presence of the Co_xFe_2 catalysts.

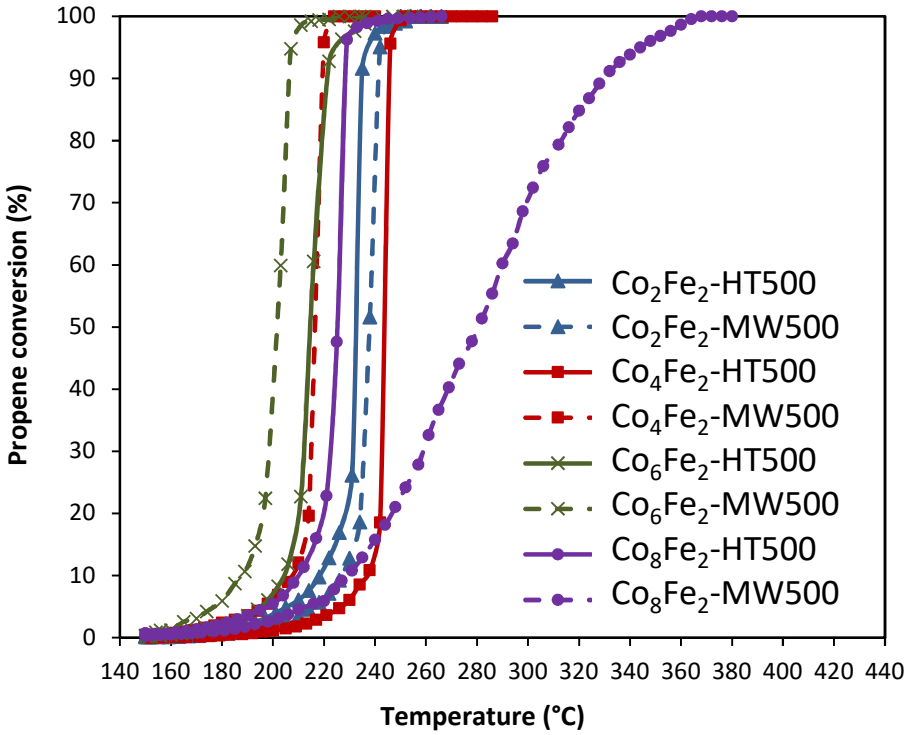

Fig. 3. Propene conversion to CO_2 versus reaction temperature on Co_xFe_2-HT500 and Co_xFe_2-MW500 samples

It should be mentioned that in all cases, the selectivity towards carbon dioxide, the desired product, is 100%. No other carbon-containing product was detected.

The classification of the catalysts is done according to the values of T_{50} (°C) reported in Table 2, corresponding to 50% of propene conversion. Firstly, for the series Co_xFe_2-HT500, the following order is obtained: Co_6Fe_2-HT500 > Co_8Fe_2-HT500> Co_2Fe_2-HT500 > Co_4Fe_2-HT500.

Among this series of catalysts, the best catalytic activity is attributed to the catalyst having a molar ratio equal to 3. Kovanda et al. [48] synthesized a series of Co-Mn-Al hydrotalcites with different molar ratios. The best activity towards ethanol oxidation was obtained for the Co_4Mn/Al sample having the highest ratio (Co + Mn). Similarly, for the decomposition of N_2O, the Co_4Mn/Al catalyst has the best catalytic performance. This result was explained by the optimal content of reducible species [48].

Concerning the series Co_xFe_2-MW500, the classification is as follows: Co_6Fe_2-MW500 > Co_4Fe_2-MW500 > Co_2Fe_2-MW500 >> Co_8Fe_2-MW500. This ranking shows that when the molar ratio increases from 1 to 3, an improvement of the catalytic performance is observed. However, when the molar ratio is equal to 4, the catalytic performance decreases significantly. Excellent activity is obtained for the catalyst Co_6Fe_2-MW500 having a molar ratio Co^{2+}/Fe^{3+} equal to 3. This catalyst gives a conversion of 100% at 212 °C.

From the T_{50} (°C) values obtained, we can establish the following global order: Co_6Fe_2-MW500 > Co_6Fe_2-HT500 = Co_4Fe_2-MW500 > Co_8Fe_2-HT500 > Co_2Fe_2-T500 ~ Co_2Fe_2-MW500 > Co_4Fe_2-HT500 >> Co_8Fe_2-MW500.
The best activity is obtained for the solid having a molar ratio equal to 3. This better activity is correlated with the greater surface area of 95 $m^2.g^{-1}$ after calcination (Table 2). Likewise, this catalyst has the easiest reducibility of the species as well as the highest experimental hydrogen consumption (Table 3).
It can be noticed that when the molar ratio is equal to 1, the two solids Co_2Fe_2-MW500 and Co_2Fe_2-HT500 showed very similar catalytic activities. When the molar ratio is equal to 2 or 3, microwave samples showed higher activities than the conventional samples. The main difference lies when the molar ratio is equal to 4, where the conventional sample Co_8Fe_2-HT500 showed higher catalytic activity than the sample Co_8Fe_2-MW500 treated under microwave. It can be deduced that both the molar ratio Co^{2+}/Fe^{3+} and the synthesis method affect the catalytic activity towards the total oxidation of propene. The synthesis using microwave irradiations thus really improves the physicochemical properties of the catalyst and consequently leads to an improvement of the catalytic activity towards the total oxidation of propene, for Co^{2+}/Fe^{3+} molar ratios equal to 2 or 3.

These results can be mainly explained by X-ray photoelectron spectroscopy (XPS).

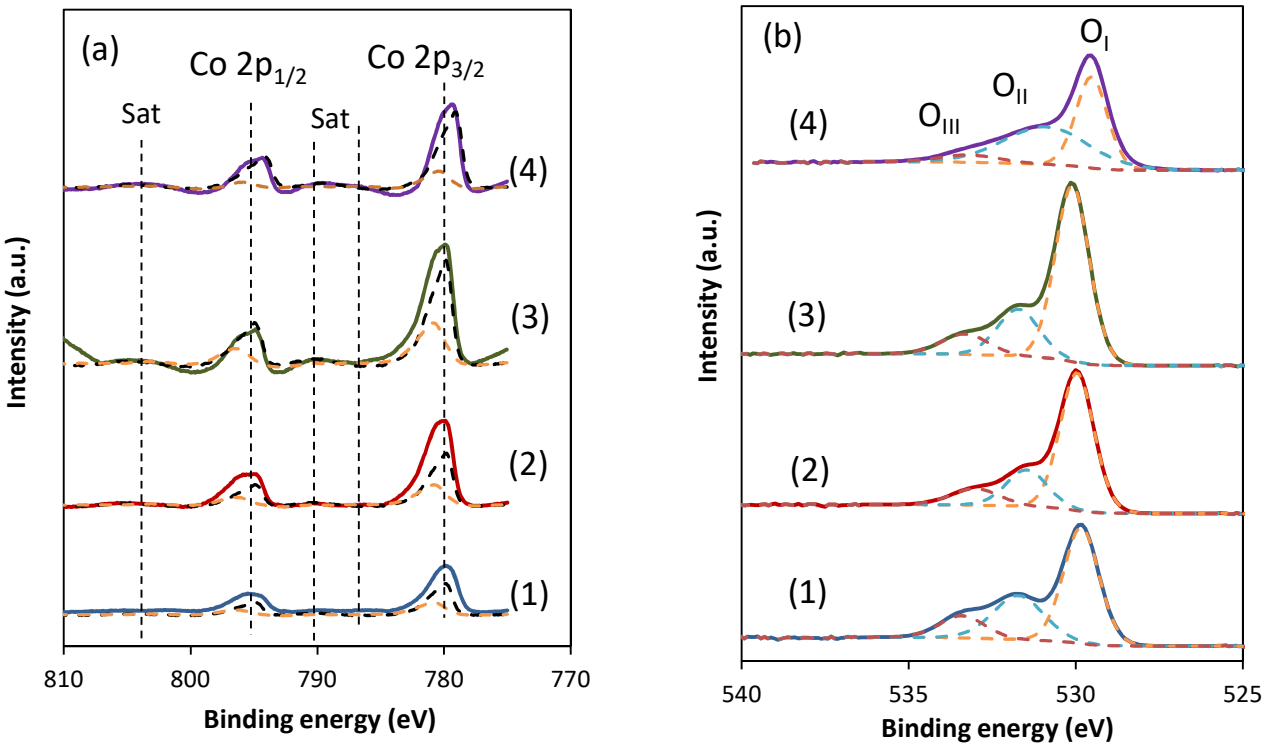

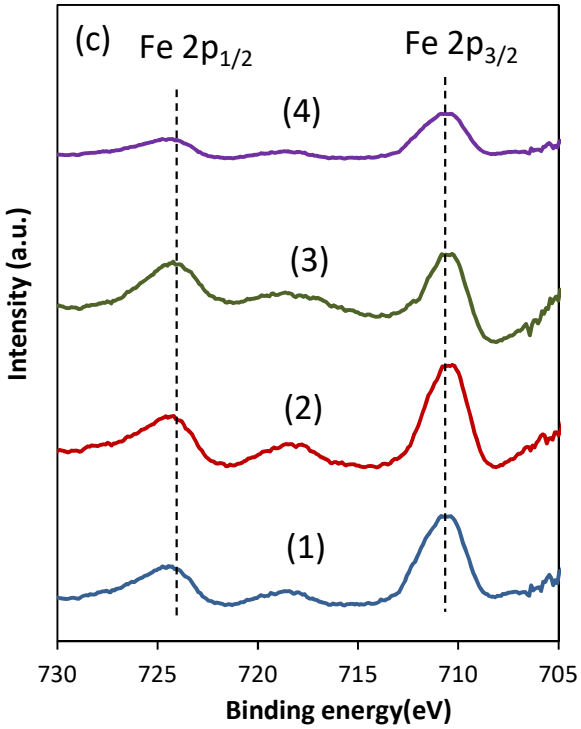

Fig. 4. XPS spectra of (a) Co 2p, (b) O 1s and (c) Fe 2p for Co_xFe_2-MW500 series. (1): Co_2Fe_2-MW500; (2): Co_4Fe_2-MW500; (3): Co_6Fe_2-MW500; (4): Co_8Fe_2-MW500

According to the XPS spectra of Co 2p in the Co_xFe_2-MW500 series with various Co/Fe molar ratios (Fig. 4(a)), two spin-orbit coupling (Co $2p_{1/2}$ and Co $2p_{3/2}$) and three satellite peaks were observed. The signals located at 796 and 780 eV correspond to the surface Co^{2+} species. However, the signals located at 794 and 779 eV correspond to the surface Co^{3+} species [49]. The Co^{3+}/Co^{2+} ratio was calculated using the relative percentage of Co^{3+} and Co^{2+} ions of the Co $2p_{3/2}$ signal. As shown in Table 4, when the molar ratio is equal to 2 or 3, the surface Co^{3+}/Co^{2+} molar ratio decreased for Co_4Fe_2-MW500 and Co_6Fe_2-MW500 compared to Co_4Fe_2-HT500 and Co_6Fe_2-HT500 respectively. Therefore, the proportion of Co^{2+} ions is higher for both microwave solids that showed better catalytic activities towards the total oxidation of propene.

Table 4. Binding energy (BE) for O 1s, Co 2p, and Fe 2p levels, relative O_{II} percentage, Co^{3+}/Co^{2+} and Co/Fe surface molar ratios for all catalysts

Catalyst	BE (O 1s) (eV)			Relative O_{II} percentage	BE (Co $2p_{1/2}$) (eV)	BE (Co $2p_{3/2}$) (eV)		Surface content Co^{3+}/Co^{2+}	BE (Fe 2p) (eV)		Co/Fe ratio
	O_I	O_{II}	O_{III}			Co^{3+}	Co^{2+}		$2p_{3/2}$	$2p_{1/2}$	
Co_2Fe_2-HT500	529.8	531.7	533.4	30.29	795.5	779.3	780.2	1.15	710.7	724	0.62
Co_2Fe_2-MW500	529.8	531.5	533	30.52	795.5	779.4	781.0	1.16	710.9	724.4	0.66
Co_4Fe_2-HT500	530	531.5	533	21.46	795.6	779.7	780.7	1.10	711	724	1.16
Co_4Fe_2-MW500	529.8	531.7	533	30.79	795.7	779.4	780.6	0.83	710.8	724	1.19
Co_6Fe_2-HT500	530.1	531.7	533.3	37.06	795.7	779.7	780.9	0.74	710.8	723.9	1.57
Co_6Fe_2-MW500	529.8	530.8	532.8	49.25	796	779.6	780.7	0.37	710.8	724	1.53
Co_8Fe_2-HT500	529.5	530.9	533.2	42.41	795.3	779.2	780.3	1.20	710.4	723.8	2.21
Co_8Fe_2-MW500	529.8	530.8	532.6	22.04	795.3	779.5	780.8	2.25	710.6	723.6	2.36

However, when the molar ratio increased to 4, the surface ratio Co^{3+}/Co^{2+} was lower for Co_8Fe_2-HT500 than for Co_8Fe_2-MW500. Co_8Fe_2-HT500 contains therefore higher proportion of Co^{2+} ions and consequently, showed better catalytic activity than the MW solid. So the best catalytic activity is correlated with the higher proportion of Co^{2+} ions.
Regarding the oxygen species, three components were observed (Fig. 4(b)). The first component (O_I) at 529 eV is attributed to oxygen species in the lattice. The second component (O_{II}) at 531 eV corresponds to surface oxygen [50]. The third component (O_{III}) at 532.5 eV corresponds to oxygen species present in carbonates and water [51]. Often the good activity of a catalytic oxidation is correlated with the surface oxygen, which presents the highest mobility among the cited oxygen species. Therefore, the relative percentages of the second component for all catalysts (O_{II}) are listed in Table 4. When the molar ratio is equal to 2 or 3, surface oxygen proportion is higher for microwave samples. So a higher proportion of surface oxygen is obtained for both microwave solids that showed better catalytic activities. When the molar ratio is equal to 4, the higher proportion of surface oxygen is obtained for the conventional solid that showed better catalytic activity than the sample treated under microwave.

Higher proportion of Co^{2+} ions on the surface and higher amount of surface oxygen are obtained for the solids Co_6Fe_2-MW500 and Co_4Fe_2-MW500 compared to Co_6Fe_2-HT500 and Co_4Fe_2-HT500 respectively. Samples Co_2Fe_2-HT500 and Co_2Fe_2-MW500, with relatively the same catalytic performances, showed approximately the same proportion of surface oxygen and Co^{2+} ions. It should be noted that all the solids of the two series Co_xFe_2-HT500 and Co_xFe_2-MW500 show a much higher activity than that

of Co_8Fe_2-MW500. The latter has the lowest catalytic activity and the lowest specific surface area of 28 $m^2.g^{-1}$ after calcination (Table 2). In addition, the lowest catalytic performance of this solid is also due to the lowest hydrogen consumption obtained in TPR.

The XPS spectra of Fe 2p in the Co_xFe_2-MW500 series presented in Fig. 4(c), showed two components Fe $2p_{3/2}$ and Fe $2p_{1/2}$ located at binding energies of 710 eV and 724 eV respectively [52]. The Co/Fe ratios on the surface of the various solids grouped in Table 4 were calculated from the Co $2p_{3/2}$ and Fe $2p_{3/2}$ signals. It should be noted that the Co/Fe surface ratio increases with the Co^{2+}/Fe^{3+} molar ratio, suggesting that the surface is rich in Co^{2+} ions. Li et al. [53] also reported an increase in the surface ratio values Co/Al with the increase of the ratio Co/Al from 1 to 5, while a further increase in the Co/Al molar ratio to 6 resulted in a decrease of Co/Al surface ratio.

3.3. Stability tests

Aging tests also called stability tests were carried out in order to give information on the lifetime of a catalyst. These tests are extremely important since the catalyst is normally used for extended hours during industrial applications.
The stability tests were carried out on the two solids Co_6Fe_2-HT500 and Co_6Fe_2-MW500 having the molar ratio Co^{2+}/Fe^{3+} equal to 3, since they have shown the highest catalytic performances for the two series Co_xFe_2-HT500 and Co_xFe_2-MW500, with $2 \leq x \leq 8$. For the sake of comparison, Co_4Fe_2-HT500 and Co_4Fe_2-MW500 catalysts were also evaluated.

In order to perform the stability tests under chemical control, low conversion percentages were chosen. Indeed, at relatively low conversions (15-20%), by-products can be formed, this fact makes it easier to detect a deactivation of the catalyst. On the other hand, at total conversion, the deactivation will be slower and more difficult to observe. Stability tests were carried out for 100 h at a fixed T_{20} temperature listed in Table 2, which corresponds to a temperature where 20% of the propene is converted.
The results of the stability tests of the two solids with a molar ratio of 2 are summarized in Fig. 5(a).

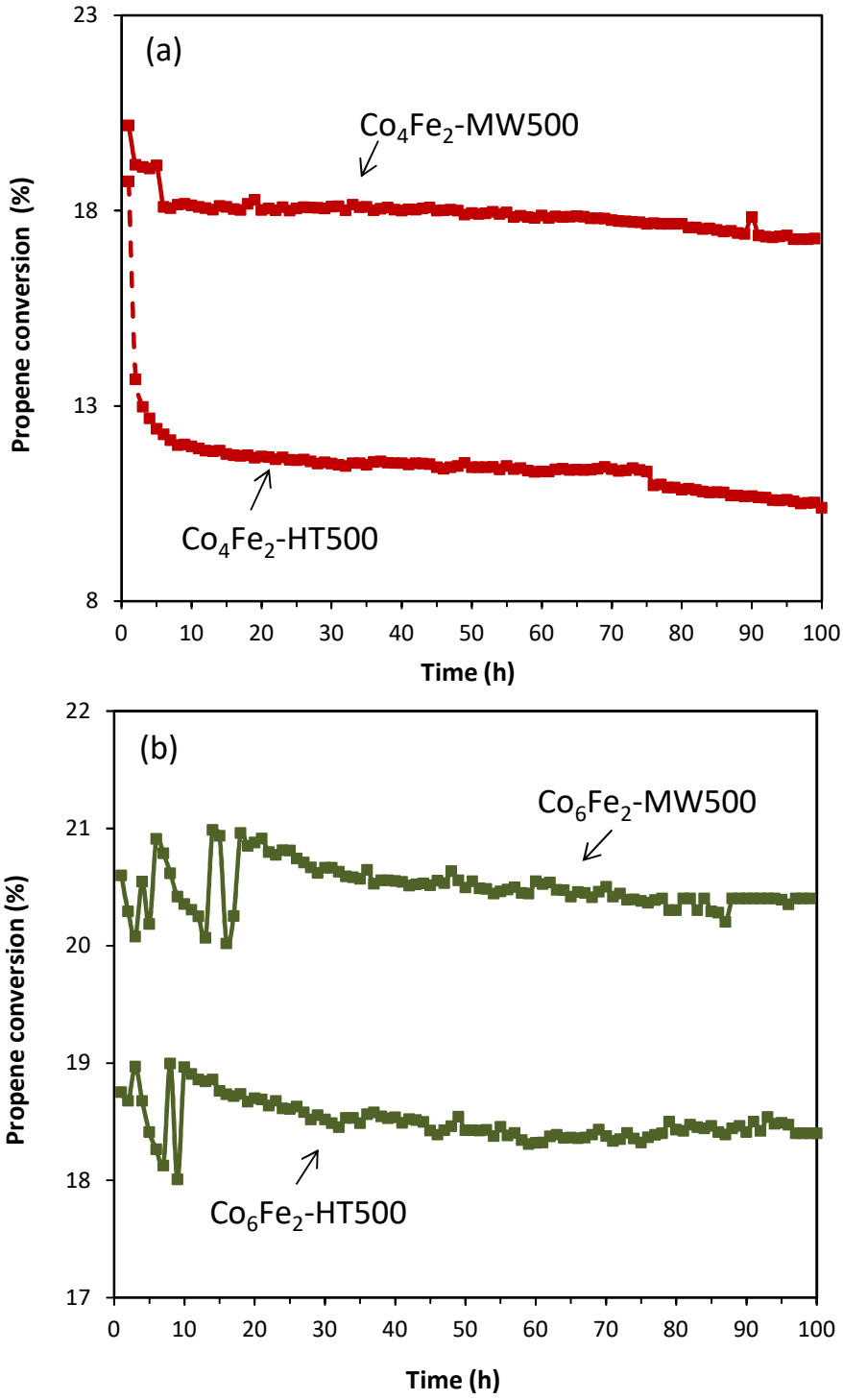

Fig. 5. Stability tests of (a) Co_4Fe_2-HT500 / Co_4Fe_2-MW500 and (b) Co_6Fe_2-HT500 / Co_6Fe_2-MW500 catalysts for 100 h

These tests were carried out at temperatures of 242 °C and 212 °C for Co_4Fe_2-HT500 and Co_4Fe_2-MW500 respectively. Indeed, a rapid fall of the conversion from the first hours of the test can be noticed. This decrease in conversion to 12% is especially noticeable for the solid Co_4Fe_2-HT500 after 10 h under flow. The latter reaches after 100 h, 10% of propene conversion. For the catalyst Co_4Fe_2-MW500, a small decrease in conversion from 20 to 18% after 10 h under flow is observed. Thus, the sample treated with microwave has a good stability under flow, better than that of the catalyst Co_4Fe_2-HT500. For Co_6Fe_2-HT500 and Co_6Fe_2-MW500, the aging tests were carried out at 209 °C and 195 °C, corresponding to a propene conversion of approximately 19 and 20% respectively (Fig. 5(b)). For the solids having a molar ratio Co^{2+}/Fe^{3+} equal to 3, an excellent and higher stability in propene conversion than those obtained for solids having a molar ratio equal to 2 is observed. This indicates that the molar ratio is important for the stability of the material. A molar ratio of 3 leads to a stability of the initial conversion, unlike the molar ratio 2. However, the catalyst Co_4Fe_2-MW500, also has a good conversion stability for long periods under flow. As a result, the Co_6Fe_2-HT500 and Co_6Fe_2-MW500 solids, and to a lesser extent the Co_4Fe_2-MW500 solid, exhibit resistance to deactivation for at least 100 h under flow.

Since carbon deposition may be one of the major catalyst aging factors, differential scanning calorimetry/thermogravimetry analyzes were performed after these stability tests. The DSC signals and the weight losses of the Co_4Fe_2 and Co_6Fe_2 solids are presented in Fig. 6 and Fig. 7 respectively.

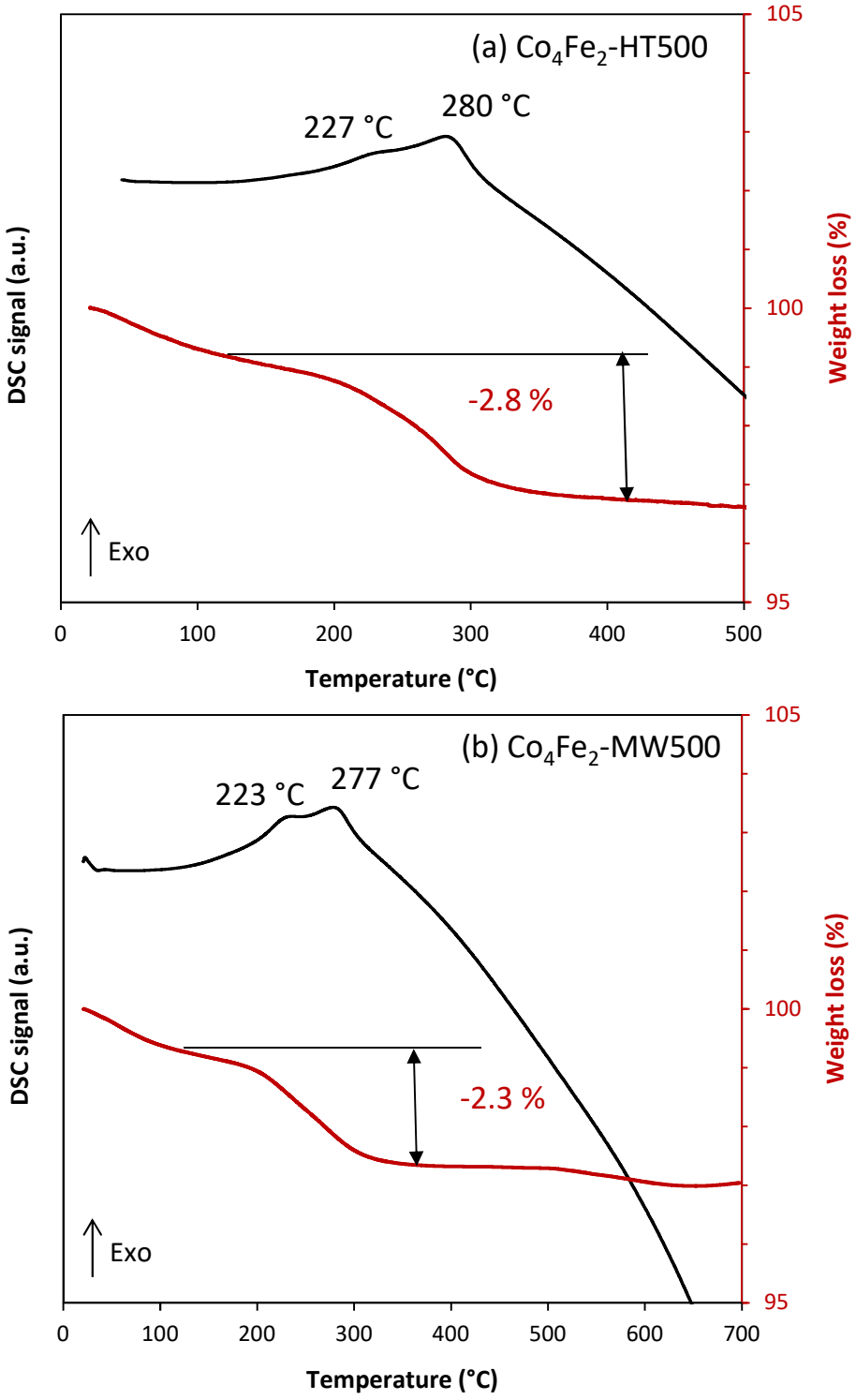

Fig. 6. Thermal analysis under air flow after stability tests of (a) Co_4Fe_2-HT500; (b) Co_4Fe_2-MW500

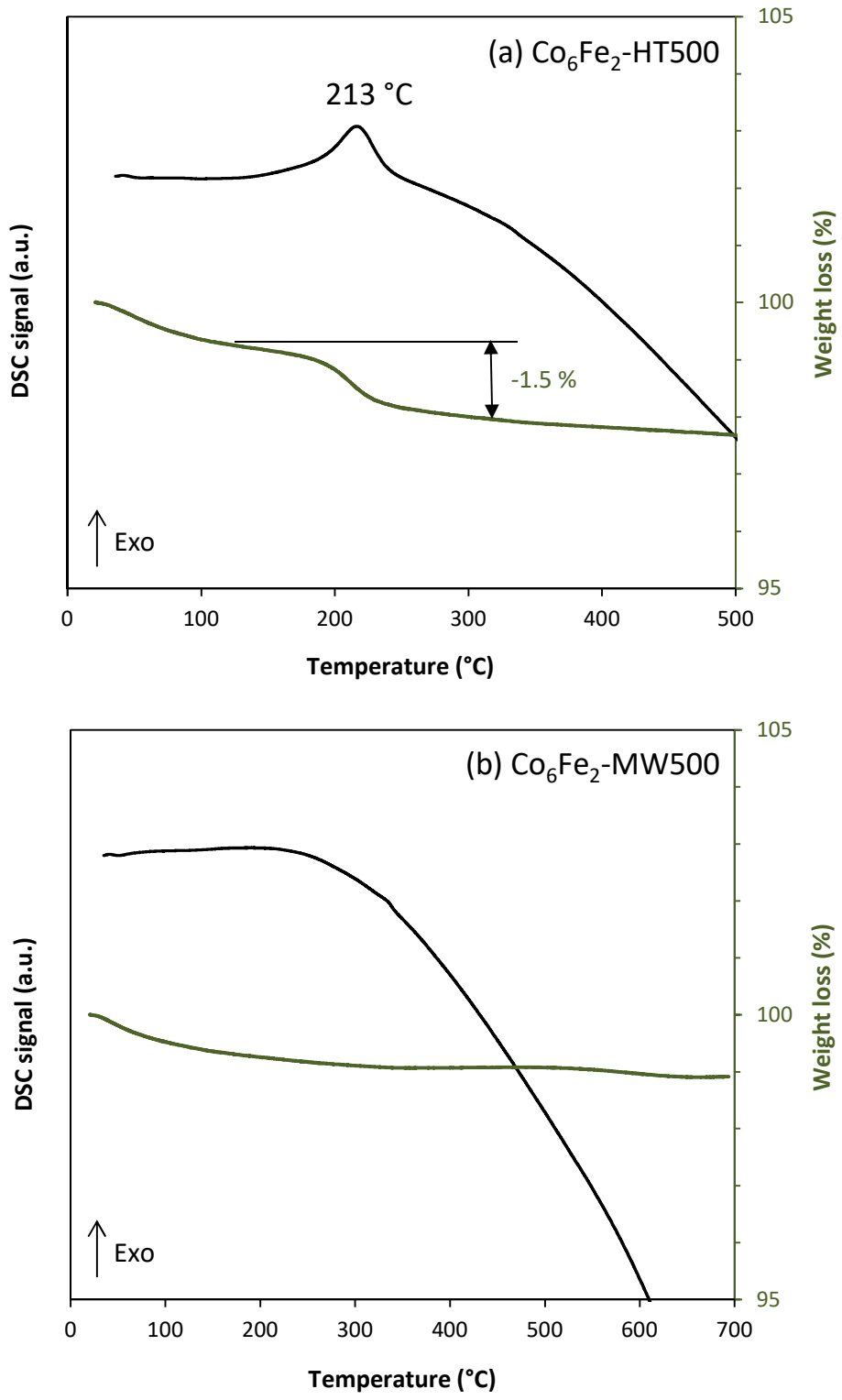

Fig. 7. Thermal analysis under air flow after stability tests of (a) Co_6Fe_2-HT500; (b) Co_6Fe_2-MW500

For the Co_4Fe_2-HT500 and Co_4Fe_2-MW500 solids, two peaks are observed at T ≤ 280 °C while for the Co_6Fe_2-HT500 catalyst a single peak is detected at 213 °C. The exothermic peaks are accompanied by a weight loss. No exothermic peak is observed for Co_6Fe_2-MW500. According to studies done by Caeiro et al. on the deactivation of H-USY zeolites [54], two types of coke can be distinguished: "light coke" and "heavy coke". The "light coke" is formed at low temperatures (< 200 °C) while the "heavy coke" is formed at high temperatures (> 350 °C) [55]. In addition, Hosseini et al. [56] identified two exothermic peaks for coke combustion over PdAu/TiO_2-ZrO_2: the first one located at 328 °C is attributed to the "light coke" oxidation and the second peak, at a higher temperature (608 °C), corresponds to the oxidation of "heavy coke" which is more difficult to oxidize.

In our case, the recorded exothermic peaks indicate that carbon residues (light coke) are formed on the surface of our catalysts. Several studies have investigated the mechanism of coke combustion [57]. At low temperatures (< 800 °C), carbon reacts with oxygen to form carbon monoxide and carbon dioxide according to the following two reactions [57,58]:

$$2\,C + O_2 \rightarrow 2\,CO$$
$$C + O_2 \rightarrow CO_2$$

The carbon monoxide formed is then oxidized according to the reaction:

$$2\,CO + O_2 \rightarrow 2\,CO_2$$

If we consider that the carbon species formed on the Co_4Fe_2 materials are oxidized at about 280 °C, temperature higher than that of total propene conversion (230 °C for Co_4Fe_2-MW500 and 250 °C for Co_4Fe_2-HT500), the coking phenomenon will take place. Furthermore, the carbon species formed on Co_6Fe_2-HT500 catalyst are oxidized at 213 °C, a temperature lower than that of total propene conversion (around 245 °C), so this catalyst is stable with time and no coking is expected to take place. Coking did not take place on Co_6Fe_2-MW500 under the studied conditions. Therefore, Co_6Fe_2-MW500 is more resistant towards deactivation by coking compared to the other studied catalysts.

3.4. Comparative study with a commercial catalyst

The catalytic performances of Co_6Fe_2 and Co_4Fe_2 series with and without microwaves irradiations were compared with that of a commercial catalyst Pd (0.5wt%)/Al_2O_3 (ACROS ORGANICS). The noble metal based catalyst is studied after calcination and after reduction. The results are shown in Fig. 8.

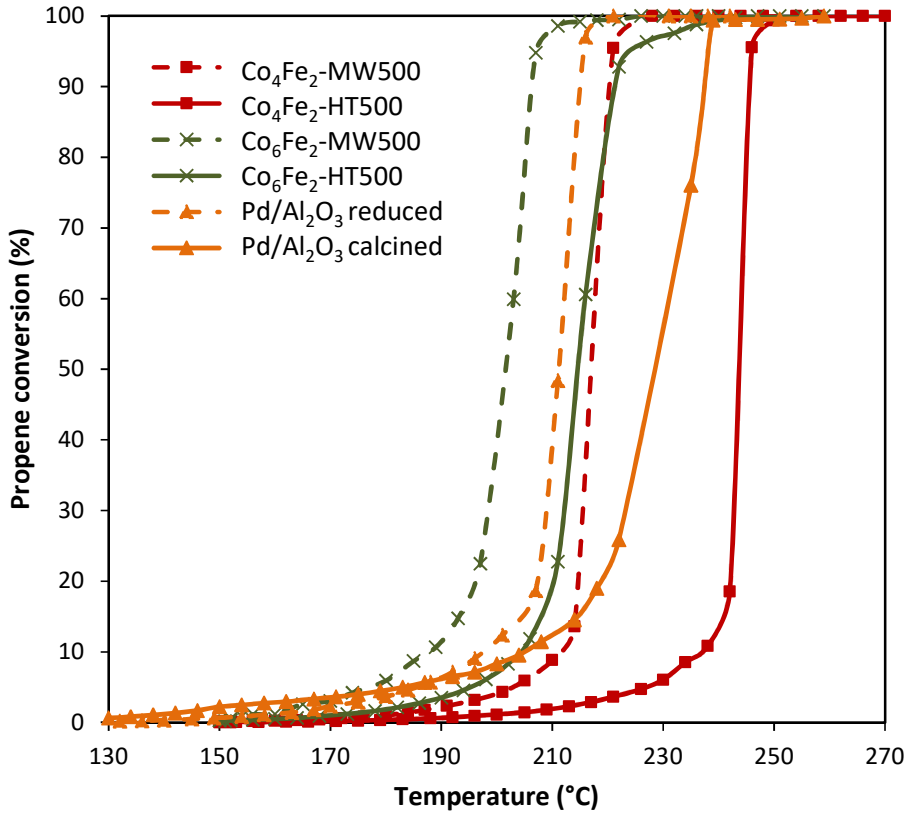

Fig. 8. Propene conversion to CO_2 versus reaction temperature on commercial $Pd(0.5\%)Al_2O_3$ catalyst and calcined Co_4Fe_2 and Co_6Fe_2 series

The Co_4Fe_2-MW500 catalyst (T_{50} = 214 °C) converts propene at lower temperatures than the calcined commercial catalyst (T_{50} = 230 °C). The commercial Pd/Al_2O_3 catalyst, previously reduced before test, is slightly better (T_{50} = 212 °C) than the Co_4Fe_2-MW500 catalyst. However, the Pd/Al_2O_3 catalyst is more expensive. In addition, the Co_6Fe_2-MW500 catalyst (T_{50} = 200 °C) exhibits higher catalytic activity than the reduced Pd/Al_2O_3 catalyst, which generally performs better than the transition metal catalysts. Thus by using microwave irradiation for the synthesis of cobalt-iron hydrotalcite materials and increasing the Co^{2+}/Fe^{3+} molar cationic ratio to 3, an excellent catalyst for propene oxidation is obtained.

It is interesting to note that in the literature, even catalysts based on calcined noble metals other than palladium show lower activities towards propene than those found in this work. Indeed, a lower activity is obtained with Au/Al_2O_3 (T_{50} = 360 °C) and $Au/xCeO_2$-Al_2O_3 (T_{50} between 265 and 235 °C) [59]. These catalysts showed an improvement in activity after reduction, as for the commercial catalyst in our case. However, their activities remain lower than those obtained with Co_6Fe_2-MW500 and even with Co_4Fe_2-MW500. Similarly, Zhang et al. [60] also tested the total oxidation of propene in the presence of the noble metal catalysts, containing 0.5% Ru and 0.5% Rh supported on TiO_2.

According to the T_{50} (°C) values, the catalytic activity obtained with 0.5% Rh/TiO_2 (T_{50} = 260 °C) is significantly lower than that of Co_4Fe_2-MW500 (T_{50} = 214 °C) and in particular that of Co_6Fe_2-MW500 (T_{50} = 200 °C). Despite the improvement in this activity by substituting rhodium with ruthenium (T_{50} = 210 °C for 0.5% Ru/TiO_2), it should be noted that this activity is almost similar to that of Co_4Fe_2-MW500 and lower than that of Co_6Fe_2-MW500.

4. Conclusion

The Co/Fe mixed metal oxides were obtained from hydrotalcite-like precursors with various Co/Fe molar ratios and different preparation methods: without (Co_xFe_2-HT) or with microwave irradiations (Co_xFe_2-MW) with $2 \leq x \leq 8$. The prepared mixed oxides were tested as catalysts in propene oxidation. It was shown that cation composition as well as microwave irradiations strongly influenced the catalytic performance of the mixed metal oxides. It was shown from the different catalytic tests carried out that the solids having the molar ratio equal to 1 do not show any significant difference between the two methods. By increasing the molar ratio to 2 and 3, the microwave method has shown a beneficial effect on the physicochemical properties of the solids. As a result, this method has made catalysts significantly more efficient than the ones prepared without microwave irradiations. However, by further increasing the molar ratio to 4, the preparation of the catalyst under microwave irradiation showed a contrary result in comparison with those of the ratios 2 and 3. In fact, with the molar ratio 4, the solid prepared by the conventional method has a significantly higher activity than the one subjected to microwave irradiations. As a result, Co_8Fe_2-MW500 gave the lowest activity towards propene oxidation. Indeed, this solid has the lowest hydrogen consumption with a very low specific surface area. Conversely, Co_6Fe_2-MW500 showed the highest catalytic activity. This better performance was ascribed to the higher specific surface area, to the relatively easy reducibility of active oxide species, to the higher proportion of mobile surface oxygen and Co^{2+} surface cations, as revealed by H_2-TPR and XPS techniques. In addition, Co_6Fe_2-MW500 showed good stability under stream and no tendency to coking as well as a better activity than a commercial 0.5wt% Pd/Al_2O_3 catalyst.

Acknowledgements

The University of Littoral – Côte d'Opale (ULCO), and the Lebanese University are gratefully acknowledged for financial supports. The authors would like to thank the Agence Universitaire de la Francophonie – Région du Moyen-Orient (AUF) and the ULCO for research fellowship. The Interreg V project "DepollutAir" (France, Wallonie, Flandres) funded by the European Union is also gratefully acknowledged for financial support. The Lebanese University is also acknowledged for financing this work through the project: "Oxydes mixtes de cobalt et de fer pour l'élimination catalytique de polluants de type composés organiques volatils (COV)."

References

[1] C. He, J. Cheng, X. Zhang, M. Douthwaite, S. Pattisson, Z. Hao, Recent Advances in the Catalytic Oxidation of Volatile Organic Compounds : A Review Based on Pollutant Sorts and Sources, Chem. Rev. 119 (2018) 4471–4568. https://doi.org/10.1021/acs.chemrev.8b00408.

[2] A.M. Carrillo, J.G. Carriazo, Cu and Co oxides supported on halloysite for the total oxidation of toluene, Appl. Catal. B Environ. 164 (2015) 443–452. https://doi.org/10.1016/j.apcatb.2014.09.027.

[3] E. Genty, S. Siffert, R. Cousin, Investigation of reaction mechanism and kinetic modelling for the toluene total oxidation in presence of CoAlCe catalyst, Catal. Today. 333 (2018) 28–35. https://doi.org/10.1016/j.cattod.2018.03.018.

[4] S. Xie, Y. Liu, J. Deng, J. Yang, X. Zhao, Z. Han, K. Zhang, H. Dai, Insights into the active sites of ordered mesoporous cobalt oxide catalysts for the total oxidation of o-xylene, J. Catal. 352 (2017) 282–292. https://doi.org/10.1016/j.jcat.2017.05.016.

[5] G. Bai, H. Dai, J. Deng, Y. Liu, F. Wang, Z. Zhao, W. Qiu, C.T. Au, Porous Co3O4 nanowires and nanorods: Highly active catalysts for the combustion of toluene, Appl. Catal. A Gen. 450 (2013) 42–49. https://doi.org/10.1016/j.apcata.2012.09.054.

[6] G. Li, C. Zhang, Z. Wang, H. Huang, H. Peng, X. Li, Fabrication of mesoporous Co3O4 oxides by acid treatment and their catalytic performances for toluene oxidation, Appl. Catal. A Gen. 550 (2018) 67–76. https://doi.org/10.1016/j.apcata.2017.11.003.

[7] Q. Yu, R. Zhuang, W. Gao, H. Yi, X. Xie, Y. Zhang, X. Tang, Mesoporous Co3O4 with large specific surface area derived from MCM-48 for catalytic oxidation of toluene, J. Solid State Chem. (2021) 122802. https://doi.org/10.1016/j.jssc.2021.122802.

[8] R. Sanchis, A. Garcia, F. Ivars-barcel, S.H. Taylor, T. Garcia, A. Dejoz, M.I. Vazquez, Sol, Highly Active Co3O4 -Based Catalysts for Total Oxidation of Light C1–C3 Alkanes Prepared by a Simple Soft Chemistry Method : Effect of the Heat-Treatment Temperature and Mixture of Alkanes, Materials (Basel). 14 (2021) 7120. https://doi.org/https://doi.org/ 10.3390/ma14237120 Academic.

[9] Q. Ren, Z. Feng, S. Mo, C. Huang, S. Li, W. Zhang, L. Chen, M. Fu, J. Wu, D. Ye, 1D-Co3O4, 2D-Co3O4, 3D-Co3O4 for catalytic oxidation of toluene, Catal. Today. 332 (2019) 160–167. https://doi.org/10.1016/j.cattod.2018.06.053.

[10] S. Dissanayake, N. Wasalathanthri, A. Shirazi Amin, J. He, S. Poges, D. Rathnayake, S.L. Suib, Mesoporous Co3O4 catalysts for VOC elimination: Oxidation of 2-propanol, Appl. Catal. A Gen. 590 (2020) 117366. https://doi.org/10.1016/j.apcata.2019.117366.

[11] J. Mei, Y. Ke, Z. Yu, X. Hu, Z. Qu, N. Yan, Morphology-dependent properties of Co3O4/CeO2 catalysts for low temperature dibromomethane (CH2Br2) oxidation, Chem. Eng. J. 320 (2017) 124–134. https://doi.org/10.1016/j.cej.2017.03.038.

[12] G.S.P. Soylu, Z. Özc, Total oxidation of toluene over metal oxides supported on a natural clinoptilolite-type zeolite, Chem. Eng. J. 162 (2010) 380–387. https://doi.org/10.1016/j.cej.2010.05.020.

[13] M. Konsolakis, S.A.C. Carabineiro, G.E. Marnellos, M.F. Asad, O.S.G.P. Soares, M.F.R. Pereira, J.J.M. Órfão, J.L. Figueiredo, Effect of cobalt loading on the solid state properties and ethyl acetate oxidation performance of cobalt-cerium mixed oxides, J. Colloid Interface Sci. 496 (2017) 141–149. https://doi.org/10.1016/j.jcis.2017.02.014.

[14] B. Solsona, T.E. Davies, T. Garcia, I. Vázquez, A. Dejoz, S.H. Taylor, Total oxidation of propane using nanocrystalline cobalt oxide and supported cobalt oxide catalysts, Appl. Catal. B Environ. 84 (2008) 176–184. https://doi.org/10.1016/j.apcatb.2008.03.021.

[15] Y. Luo, Y. Zheng, J. Zuo, X. Feng, X. Wang, T. Zhang, Insights into the high performance of Mn-Co oxides derived from metal- organic frameworks for total toluene oxidation, J. Hazard. Mater. 349 (2018) 119–127. https://doi.org/10.1016/j.jhazmat.2018.01.053.

[16] B. Solsona, T. García, R. Sanchis, M.D. Soriano, M. Moreno, E. Rodríguez-Castellón, S. Agouram, A. Dejoz, J.M. López Nieto, Total oxidation of VOCs on mesoporous iron oxide catalysts: Soft chemistry route versus hard template method, Chem. Eng. J. 290 (2016) 273–281. https://doi.org/10.1016/j.cej.2015.12.109.

[17] T.K. Tseng, H.U. Chu, The kinetics of catalytic incineration of styrene over a MnO/Fe2O3 catalyst, Sci. Total Environ. 275 (2001) 83–93. https://doi.org/10.1016/S0048-9697(00)00856-1.

[18] S.C. Kim, W.G. Shim, Influence of physicochemical treatments on iron-based spent catalyst for catalytic oxidation of toluene., J. Hazard. Mater. 154 (2008) 310–6. https://doi.org/10.1016/j.jhazmat.2007.10.027.

[19] F.G.E. Nogueira, J.H. Lopes, A.C. Silva, R.M. Lago, J.D. Fabris, L.C.A. Oliveira, Catalysts based on clay and iron oxide for oxidation of toluene, Appl. Clay Sci. 51 (2011) 385–389. https://doi.org/10.1016/j.clay.2010.12.007.

[20] D. Li, C. Li, K. Suzuki, Catalytic oxidation of VOCs over Al- and Fe-pillared montmorillonite, Appl. Clay Sci. 77–78 (2013) 56–60. https://doi.org/10.1016/j.clay.2013.02.027.

[21] C.A. Serhal, I. Mallard, C. Poupin, M. Labaki, S. Siffert, R. Cousin, Ultraquick synthesis of hydrotalcite-like compounds as efficient catalysts for the oxidation of volatile organic compounds, Comptes Rendus Chim. 21 (2018) 993–1000. https://doi.org/10.1016/j.crci.2018.09.012.

[22] M.J. Wu, J.Z. Wu, J. Zhang, H. Chen, J.Z. Zhou, G.R. Qian, Z.P. Xu, Z. Du, Q.L. Rao, A review on fabricating heterostructures by layered double hydroxides for enhanced photocatalytic activities, Catal. Sci. Technol. 8 (2018) 1207–1228. https://doi.org/10.1039/C7CY02314F.

[23] E. Genty, J. Brunet, C. Poupin, S. Casale, S. Capelle, P. Massiani, S. Siffert, R. Cousin, Co-Al mixed oxides prepared via LDH route using microwaves or

ultrasound: Application for catalytic toluene total oxidation, Catalysts. 5 (2015) 851–867. https://doi.org/10.3390/catal5020851.

[24] C.A. Serhal, I. Mallard, C. Poupin, M. Labaki, S. Siffert, R. Cousin, Effect of Microwave Irradiation Parameters on Co/Fe Hydrotalcite Nanocatalysts for the Total Oxidation of VOCs, Eur. J. Inorg. Chem. 2019 (2019) 3218–3227. https://doi.org/10.1002/ejic.201801528.

[25] F. Cavani, F. Trifirò, A. Vaccari, Hydrotalcite-type anionic clays: Preparation, properties and applications., Catal. Today. 11 (1991) 173–301. https://doi.org/10.1016/0920-5861(91)80068-K.

[26] M. V. Bukhtiyarova, A review on effect of synthesis conditions on the formation of layered double hydroxides, J. Solid State Chem. 269 (2019) 494–506. https://doi.org/10.1016/j.jssc.2018.10.018.

[27] M. Haraketi, K. Hosni, E. Srasra, Intercalation behavior of salicylic acid into calcined for Cu-Al-layered double hydroxides for a controlled release Formulation, Surf. Eng. Appl. Electrochem. 53 (2017) 360–370. https://doi.org/10.3103/S106837551704007X.

[28] K. Abderrazek, N.F. Srasra, E. Srasra, Synthesis and Characterization of [Zn-Al] Layered Double Hydroxides: Effect of the Operating Parameters Kaouther Abderrazek, J. Chinese Chem. Soc. 64 (2017) 1–8. https://doi.org/10.1002/jccs.201600258.

[29] A. Ahmed Ali Ahmed, Z. Abidin Talib, M. Zobir bin Hussein, A. Zakaria, Zn–Al layered double hydroxide prepared at different molar ratios: Preparation, characterization, optical and dielectric properties, J. Solid State Chem. 191 (2012) 271–278. https://doi.org/10.1016/j.jssc.2012.03.013.

[30] T. Ishikawa, K. Matsumoto, K. Kandori, T. Nakayama, Synthesis of layered zinc hydroxide chlorides in the presence of Al(III), J. Solid State Chem. 179 (2006) 1110–1118. https://doi.org/10.1016/j.jssc.2006.01.007.

[31] A.H. Iglesias, O.P. Ferreira, D.X. Gouveia, A.G. Souza, A.C. De Paiva, Structural and thermal properties of Co–Cu–Fe hydrotalcite-like compounds, J. Solid State Chemsitry. 178 (2005) 142–152. https://doi.org/10.1016/j.jssc.2004.10.039.

[32] K. Ma, J.P. Cheng, J. Zhang, M. Li, F. Liu, X. Zhang, Dependence of Co/Fe ratios in Co-Fe layered double hydroxides on the structure and capacitive properties, Electrochim. Acta. 198 (2016) 231–240. https://doi.org/10.1016/j.electacta.2016.03.082.

[33] C. Gennequin, S. Kouassi, L. Tidahy, R. Cousin, J.F. Lamonier, G. Garcon, P. Shirali, F. Cazier, A. Aboukaïs, S. Siffert, Co-Mg-Al oxides issued of hydrotalcite precursors for total oxidation of volatile organic compounds. Identification and toxicological impact of the by-products, Comptes Rendus Chim. 13 (2010) 494–501. https://doi.org/10.1016/j.crci.2010.01.001.

[34] R. Mrad, R. Cousin, C. Poupin, A. Aboukaïs, S. Siffert, Propene oxidation and NO reduction over MgCu-Al(Fe) mixed oxides derived from hydrotalcite-like compounds, Catal. Today. 257 (2015) 98–103.

https://doi.org/10.1016/j.cattod.2015.02.020.

[35] M.E. Pérez Bernal, R.J.R. Casero, V. Rives, Preparation and properties of Co-Fe mixed oxides obtained by calcination of layered double hydroxides, Ceramics-Silikaty. 48 (2004) 145–154.

[36] S. Kannan, S. Velu, V. Ramkumar, C.S. Swamy, Synthesis and physicochemical properties of cobalt aluminium hydrotalcites, J. Mater. Sci. 30 (1995) 1462–1468. https://doi.org/10.1007/BF00375249.

[37] M. Herrero, P. Benito, F.M. Labajos, V. Rives, Nanosize cobalt oxide-containing catalysts obtained through microwave-assisted methods, Catal. Today. 128 (2007) 129–137. https://doi.org/10.1016/j.cattod.2007.06.070.

[38] F. Leroux, E.M. Moujahid, C. Taviot-Guého, J.-P. Besse, Effect of layer charge modification for Co-Al layered double hydroxides: Study by X-ray absorption spectroscopy, Solid State Sci. 3 (2001) 81–92. https://doi.org/10.1016/S1293-2558(00)01119-5.

[39] E. Scavetta, B. Ballarin, M. Gazzano, D. Tonelli, Electrochimica Acta Electrochemical behaviour of thin films of Co/Al layered double hydroxide prepared by electrodeposition, Electrochim. Acta. 54 (2009) 1027–1033. https://doi.org/10.1016/j.electacta.2008.07.078.

[40] V. Rives, A. Dubey, S. Kannan, Synthesis, characterization and catalytic hydroxylation of phenol over CuCoAl ternary hydrotalcites, Phys. Chem. Chem. Phys. 3 (2001) 4826–4836. https://doi.org/10.1039/B103656B.

[41] A. Biabani-ravandi, M. Rezaei, Low temperature CO oxidation over Fe-Co mixed oxide nanocatalysts, Chem. Eng. J. 184 (2012) 141–146. https://doi.org/10.1016/j.cej.2012.01.017.

[42] D.C. Carvalho, N.A. Ferreira, J.M. Filho, O.P. Ferreira, J.M. Soares, A.C. Oliveira, Ni–Fe and Co–Fe binary oxides derived from layered double hydroxides and their catalytic evaluation for hydrogen production, Catal. Today. 250 (2015) 155–165. https://doi.org/10.1016/j.cattod.2014.08.010.

[43] Y. Ji, Z. Zhao, A. Duan, G. Jiang, J. Liu, Comparative Study on the Formation and Reduction of Bulk and Al2O3-Supported Cobalt Oxides by H2-TPR Technique, J. Phys. Chem. 113 (2009) 7186–7199. https://doi.org/10.1021/jp8107057.

[44] D. Klissurski, E. Uzunova, K. Ivanov, Binary spinel cobaltites of nickel, copper and zinc as precursors of catalysts for carbon oxides methanation, Catal. Letters. 15 (1992) 385–391. https://doi.org/10.1007/BF00769162.

[45] Y. Hammiche-Bellal, N. Zouaoui-Mahzoul, I. Lounas, Cobalt and cobalt-iron spinel oxides as bulk and silica supported catalysts in the ethanol combustion reaction, J. Mol. Catal. A Chem. 426 (2017) 97–106. https://doi.org/10.1016/j.molcata.2016.11.005.

[46] E. Manova, T. Tsoncheva, C. Estournès, D. Paneva, K. Tenchev, I. Mitov, L. Petrov, Nanosized iron and iron–cobalt spinel oxides as catalysts for methanol decomposition, Appl. Catal. A, Gen. 300 (2006) 170–180. https://doi.org/10.1016/j.apcata.2005.11.005.

[47] M. Arco, R. Trujillano, V. Rives, Cobalt–iron hydroxycarbonates and their evolution to mixed oxides with spinel structure, J. Mater. Chem. 8 (1998) 761–767. https://doi.org/10.1039/A705503J.

[48] F. Kovanda, T. Rojka, J. Dobesova, V. Machovic, P. Bezdickac, L. Obalova, K. Jiratova, T. Grygar, Mixed oxides obtained from Co and Mn containing layered double hydroxides: Preparation , characterization , and catalytic properties, J. Solid State Chem. 179 (2006) 812–823. https://doi.org/10.1016/j.jssc.2005.12.004.

[49] B. Bai, J. Li, Positive Effects of K ions on Three-Dimensional Mesoporous Ag/Co3O4 Catalyst for HCHO Oxidation, Am. Chem. Soc. 4 (2014) 2753–2762. https://doi.org/10.1021/cs5006663.

[50] Y. Sun, N. Li, X. Xing, X. Zhang, Z. Zhang, G. Wang, J. Cheng, Z. Hao, Catalytic oxidation performances of typical oxygenated volatile organic compounds (acetone and acetaldehyde) over MAlO (M = Mn, Co, Ni, Fe) hydrotalcite-derived oxides, Catal. Today. 327 (2019) 389–397. https://doi.org/10.1016/j.cattod.2018.03.002.

[51] J. Luo, M. Meng, X. Li, X. Li, Y. Zha, T. Hu, Mesoporous Co3O4 – CeO2 and Pd/Co3O4–CeO2 catalysts: Synthesis, characterization and mechanistic study of their catalytic properties for low-temperature CO oxidation, J. Catal. 254 (2008) 310–324. https://doi.org/10.1016/j.jcat.2008.01.007.

[52] X. Zhang, Y. Wang, S. Dong, M. Li, Dual-site polydopamine spheres/CoFe layered double hydroxides for electrocatalytic oxygen reduction reaction, Electrochim. Acta. 170 (2015) 248–255. https://doi.org/10.1016/j.electacta.2015.04.170.

[53] D. Li, Y. Ding, X. Wei, Y. Xiao, L. Jiang, Cobalt-aluminum mixed oxides prepared from layered double hydroxides for the total oxidation of benzene, Appl. Catal. A Gen. 507 (2015) 130–138. https://doi.org/10.1016/j.apcata.2015.09.038.

[54] G. Caeiro, J.M. Lopes, P. Magnoux, P. Ayrault, F.R. Ribeiro, A FT-IR study of deactivation phenomena during methylcyclohexane transformation on H-USY zeolites: Nitrogen poisoning, coke formation, and acidity–activity correlations, J. Catal. 249 (2007) 234–243. https://doi.org/10.1016/j.jcat.2007.04.005.

[55] M. Guisnet, P. Magnoux, Organic chemistry of coke formation, Appl. Catal. A Gen. 212 (2001) 83–96. https://doi.org/10.1016/S0926-860X(00)00845-0.

[56] M. Hosseini, S. Siffert, R. Cousin, A. Aboukaïs, Z. Hadj-Sadok, B.-L. Su, Total oxidation of VOCs on Pd and/or Au supported on TiO2/ ZrO2 followed by “operando” DRIFT, Comptes Rendus Chim. 12 (2009) 654–659. https://doi.org/10.1016/j.crci.2008.09.032.

[57] P. Basu, J. Broughton, D.E. Elliott, Combustion of single coal particles in fluidised beds, Inst. Fuel Symp. Ser. 1 (1975) A3.

[58] S. Slaoui, T. Bounahmidi, Étude Expérimentale Et Modélisation De La Cinétique De Combustion Du Coke, Comptes Rendus Chim. 7 (2004) 547–557. https://doi.org/10.1016/j.crci.2004.01.010.

[59] P. Lakshmanan, L. Delannoy, V. Richard, C. Méthivier, C. Potvin, C. Louis, Total

oxidation of propene over Au/xCeO2-Al2O3 catalysts: Influence of the CeO2 loading and the activation treatment, Appl. Catal. B Environ. 96 (2010) 117–125. https://doi.org/10.1016/j.apcatb.2010.02.009.

[60] Z. Zhang, M. Chen, W. Shangguan, Low-temperature SCR of NO with propylene in excess oxygen over the Pt/TiO2 catalyst, Catal. Commun. 10 (2009) 1330–1333. https://doi.org/10.1016/j.catcom.2009.02.015.

List of figures

List of tables

Graphical abstract

Influence of Co/Fe molar ratio on hydrotalcite catalysts prepared with or without microwave

Cynthia Abou Serhal[a,b], Rebecca El Khawaja[a], Madona Labaki[b], Isabelle Mallard[a], Christophe Poupin[a], Renaud Cousin[a*], Stéphane Siffert[a*]

a Université du Littoral Côte d'Opale (ULCO), Unité de Chimie Environnementale et Interactions sur le Vivant (UCEIV, U.R. 4492), SFR Condorcet FR CNRS 3417, MREI, F-59140 Dunkerque, France

b Lebanese University, Laboratory of Physical Chemistry of Materials (LCPM)/PR2N, Faculty of Sciences, Fanar, P.O. Box 90656, Jdeidet El Metn, Lebanon

* Corresponding authors. E-mail addresses: stéphane.siffert@univ-littoral.fr; renaud.cousin@univ-littoral.fr; Tel.: +33-03-2865-8256; +33-03-2865-8276.